Experimental verification of near-wall hindered diffusion for the Brownian motion of nanoparticles using evanescent wave microscopy

Arindam Banerjee[1] and Kenneth D. Kihm[2,*]
[1]*Department of Mechanical Engineering, Texas A&M University, College Station, Texas 77843, USA*
[2]*Department of Mechanical, Aerospace and Biomedical Engineering, University of Tennessee, Knoxville, Tennessee 37996, USA*
(Received 17 June 2005; published 28 October 2005)

A total internal reflection fluorescence microscopy technique coupled with three-dimensional tracking of nanoparticles is used to experimentally verify the theory on near-wall hindered Brownian motion [Goldman *et al.*, Chem. Eng. Sci. **22**, 637 (1967); Brenner, Chem. Eng. Sci. **16**, 242 (1967)] very close to the solid surface (within ~ 1 μm). The measured mean square displacements (MSDs) in the lateral x-y directions show good agreement with the theory for all tested nanoparticles of radii 50, 100, 250, and 500 nm. However, the measured MSDs in the z direction deviate substantially from the theory particularly for the case of smaller particles of 50 and 100 nm radius. Since the theory considers only the hydrodynamic interaction of moving particles with a stationary solid wall, additionally possible interaction forces like gravitational forces, van der Waals forces, and electro-osmotic forces have been examined to delineate the physical reasons for the discrepancy.

DOI: 10.1103/PhysRevE.72.042101 PACS number(s): 05.40.Jc, 47.15.Pn, 78.67.Bf, 83.10.Mj

Total internal reflection fluorescence microscopy (TIRFM), also know as evanescent wave microscopy, has been used in observing secretory granules in cells as they approach within a few hundred nanometers of the cell boundary or membrane [1]. This technique has also been used by colloidal chemists to monitor the instantaneous separation distance of a microsphere (>1 μm) from a flat plate [2]. The evanescent wave decays exponentially with the elevation of the sphere and the amount of light scattered by the sphere is analyzed to determine its elevation. More recently, the scope of TIRFM has been broadened to dynamically track far smaller nanoparticles suspended in the flow region extremely close to a solid surface [3,4]. Using a ratiometric concept for TIRFM [3,5], three-dimensional detection of Brownian motion has been achieved for 100-nm-radius particles suspended in water. The normal component ($D_\perp$) of the measured Brownian diffusivity shows substantial deviation from the early developed theory for near-wall hindered Brownian diffusion [6–8] while the lateral components ($D_\parallel$) show good agreement with the theory.

This paper presents our experimental and analytical attempts to explore the physics that can explain the discrepancies. The measurements for three-dimensional Brownian motions have been extended for four different monodispersed batches of nanoparticles with different radii from 50 to 500 nm. Various short- and long-range interactions between the particles and the solid surface, including the gravitational potential, van der Waals potential, and electrostatic potential due to the electro-osmotic forces, have been examined to determine the discrepancy of the data from the overly simplified theory. Understanding particle-particle and particle-wall interactions allows us to control equilibrium self-assembly of colloidal structures on substrates that is crucial to numerous complex fluid and advanced material technologies.

The Stokes-Einstein diffusion theory [9] assumes spherical particles in a dilute suspension of an identical specific gravity so that their diffusivity can be calculated solely from the balance of the thermal kinetic motion with the viscous drag force, i.e., the Stokes law

$$D_0 = \frac{kT}{6\pi\mu a} M^0 \tag{1}$$

where k is the Boltzmann constant, T the suspension temperature in absolute Kelvin scale, μ the dynamic viscosity of the fluid, and M^0 represents a unit tensor of 3×3 elements for the free or unhindered Brownian motion. However, when particles are present very close to a solid wall, the Brownian motion can be substantially hindered. The dynamics of the particles close to the wall become significantly non-Gaussian and the average particle displacement can differ from the random and isotropic most probable displacement. The presence of the anisotropic solid boundary at a finite distance necessitates corrections to Eq. (1). Thus a near-wall "hindered" diffusion coefficient, the free diffusion unit tensor M^0, is substituted by the hindered diffusion tensor M^H.

$$D_H = \frac{kT}{6\pi\mu a} M^H, \tag{2}$$

where $M^H=[\lambda_{ij}]$, $\lambda_{ij}=0\ \forall\ i\neq j$, $\lambda_{11}=\lambda_{22}=\lambda_\parallel$, and $\lambda_{33}=\lambda_\perp$. Goldman *et al.* [6] analyzed the slow viscous motion of a sphere in a quiescent viscous fluid and used an asymptotic solution of the Stokes equation to analyze rotational and translational motion close to the wall. The hindered motion is incorporated to the Stokes drag increase, and thus leads to the reduction of the Brownian diffusivity. He deduced a correction term to account for the hindered particle movement parallel to the plane wall as

$$\lambda_\parallel = \left(1 - \frac{9}{16}\Lambda + \frac{1}{8}\Lambda^3 - \frac{45}{256}\Lambda^4 - \frac{1}{16}\Lambda^5\right)^{-1} \tag{3}$$

where $\Lambda = a/(a+h)$. Brenner [7] provided an analytical expression in the form of an infinite series to account for the

*Email address: kkihm@utk.edu

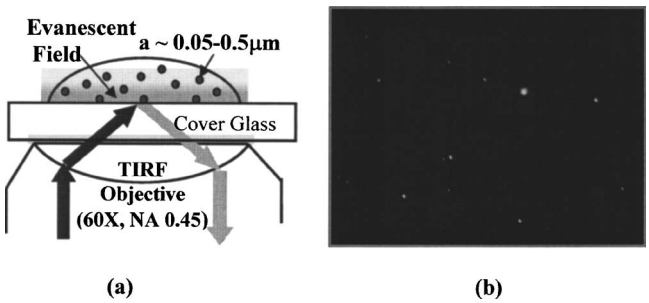

FIG. 1. (a) Operating principle of high-numerical-aperture (oil-immersion type) objective based TIRFM. The penetration depth z_p of the evanescent wave is 272 nm. (b) 100-nm-radius nanoparticles at the illumination conditions described in (a).

correction term for motion normal to the surface. An approximation [8] has been derived from a regression of the infinite series expression to derive the hindered diffusion tensor in the normal direction as

$$\lambda_{\perp} = \frac{6h^2 + 2ah}{6h^2 + 9ah + 2a^2}. \tag{4}$$

Based on our literature survey, the hindered diffusion theory is yet to be experimentally examined for the case of nanoparticles. The ratiometric TIRFM technique [1,5] allows three-dimensional tracking of nanoparticles in the submicrometer region from a solid surface so that experimental determination of $\lambda_{\parallel}$ and $\lambda_{\perp}$, and hence $D_{\perp}$ and $D_{\parallel}$, can be possible. Tested nanoparticles are yellow-green (505 nm/515 nm) carboxylate coated fluorescent spherical beads in four different sizes of 50, 100, 250, and 500 nm radii, with less than ±5% variations in their radii. The polystyrene spheres have a specific gravity of 1.055 and carry weak negative charges because of their $COOH^-$ group attached to carboxylate. The evanescent wave field is generated by an argon-ion laser tuned at 488 nm fed into a 60×, 1.45NA TIRF lens (Fig. 1). Monodispersed nanoparticles are tracked over a span of 120 images to determine the mean square displacement (MSD). The MSD of each component (x, y, or z) is defined as two times the Brownian diffusivity weighted by the time increment between two successive imaging frames, i.e., $2D_H\Delta t$. The measured values of the lateral MSD components, $\langle x^2\rangle$ or $\langle y^2\rangle$, agree well with the theoretical predictions (Fig. 2). The theoretical curves represent the average hindrance values for the region spanning from $h=0$ to $2z_p$ with z_p being the evanescent penetration depth at which its intensity decreases to e^{-1} from the initial illumination intensity at the glass substrate–fluid interface. Small discrepancy is observed only for the case of the 50 nm radius, but the discrepancy is within the experimental uncertainty represented by the extended error bar. However, the normal component $\langle z^2\rangle$ deviates from the theory showing progressively substantial underestimation with decreasing particle sizes, particularly for 100 and 50 nm particles, whereas $\langle z^2\rangle$ measurements for the bigger 250 and 500 nm particles show good agreement with the theory. We were intrigued by the persistently underestimated z-component MSD data observed for the smaller nanoparticles.

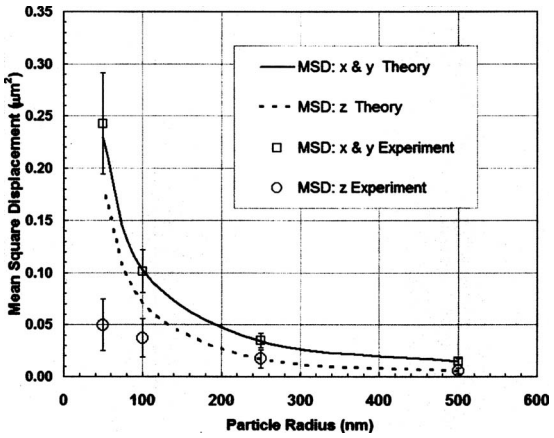

FIG. 2. Comparison of the measured mean square displacement (MSD) values with predictions based on the theory [6,7] accounting for only the hydrodynamic particle-wall interactions.

In addition to the hydrodynamic interaction between a neutrally buoyant single sphere and the wall, at least four additional effects can be considered, namely, particle-to-particle interactions, sedimentation, electrostatic and electro-osmotic forces, and short-range van der Waals forces between the suspended particles and the glass wall. The remainder of the Brief Report presents examinations of these factors for their possible alteration of the hindered Brownian motion beyond the hydrodynamic effect. The extremely low volume fraction of 0.001% used for our experiments provides the average interparticle distance being larger than 100 times their radius, so that the resulting interparticle effect could be considered negligible [10,11]. The next concern is the effect of particle sedimentation due to the density mismatch between the tested nanoparticles (specific gravity 1.055) and water. The ratio of the gravitational to the diffusive forces of a freely suspended sphere gives the effective sedimentation measure as dimensionless Péclet number Pe:

$$\mathrm{Pe} = \frac{Lu_{sed}}{D_H} = \frac{4\pi a^3 \Delta\rho g}{9\mu D_H} \tag{5}$$

where the system length L is set to the particle diameter $2a$. The correction coefficient for the sedimentation speed (u_{sed}) based on the volume fraction is about 0.995 given the present low volume concentration, and the sedimentation speed is assumed identical to the terminal velocity [12]. Table I shows the sedimentation speeds, the Reynolds numbers, and the Péclet numbers that are all very low for the four tested particles. In particular, the low Péclet numbers imply negli-

TABLE I. Sedimentation velocity (u_{sed}), Reynolds number (Re), and Péclet Number (Pe) for nanospheres of radius a.

a (nm)	U_{sed}(m/s)	Re	Pe
500	2.73×10^{-8}	1.43×10^{-8}	0.03896
250	6.81×10^{-9}	1.79×10^{-9}	0.00789
100	1.09×10^{-9}	1.14×10^{-10}	0.00099
50	2.73×10^{-10}	1.43×10^{-11}	0.00021

gibly small gravitational sedimentation to occur.

The time-independent interactions between a sphere and a substrate surface refer to the gravitational forces, the van der Waals forces, and the electrical double layer forces. Thus, the total potential energy carried by a particle located at height h, measured from the substrate surface, is given by

$$\phi(h) = \phi_g(h) + \phi_{VdW}(h) + \phi_e(h). \quad (6)$$

The gravitational potential $\phi_g(h)$ under a constant gravity is expressed as

$$U_g(h) = F_g h = \frac{4}{3}\pi a^3 g \Delta\rho h. \quad (7)$$

Another contribution to the total potential comes from the short-ranged dispersion interaction that becomes more important with increasing particle concentrations [12]. For the present low 0.001% volume fraction, we take Hamaker's linearized superposition formula assuming negligibly small particle-to-particle interactive forces [13]. The van der Waals potential $\phi_{VdW}(h)$ is thus given by

$$\phi_{VdW} = -\frac{A_{123}}{6kT}\left[\frac{1}{\delta} + \frac{1}{\delta+2} + \ln\left(\frac{\delta}{\delta+2}\right)\right], \quad (8)$$

where $\delta = h/a$, and A_{123} represents the Hamaker constant for sphere (1) immersed in water (2) with a glass (3) substrate. For the case of larger particles on the order of micrometers, Bevan and Prieve [8] successfully used this formula to interpret the sphere-wall interaction potentials. Analytical expressions for the electrostatic forces and free energies of interaction for spherical particles are available as the linear superposition approximation, which is valid when the particles are far apart and the double layer overlapping is relatively weak. Alternatively, one can use the Derjaguin approximation for thin double layers relative to the particle size [2] to derive the free energy between a sphere and a planar wall. The electrical double layer interactions can also be obtained by superimposing the electrostatic potential profile that is derived from the nonlinear Poisson-Boltzmann equation considering two isolated plane double layers, and then applying Derjaguin's approximation to analogously calculate the interaction forces between two spherical double layers. Part of the difficulty of calculating the forces and interaction-free energies is due to the nonlinear nature of the Poisson-Boltzmann theory that renders the problem analytically intractable except for the simplest geometries.

Recent studies [2,14] have derived analytical expressions for sphere-wall interactions for various boundary conditions. Based on the Derjaguin approximation, we use a constant charge model, i.e., particles which maintain a uniform fixed surface charge density during interaction. The electrostatic potential $\phi_e(h)$ on the plate is then given by [2]

$$\phi_e(h) = 16\varepsilon a\left(\frac{kT}{e}\right)^2 \tanh\left(\frac{e\psi_1}{4kT}\right)\tanh\left(\frac{e\psi_2}{4kT}\right)e^{-\kappa h} \quad (9)$$

where ψ_1 and ψ_2 are the Stern potentials of the substrate surface (1) and the particle surface (2), respectively, ε is the dielectric permittivity of water, e is the elemental electric charge, and κ is the Debye-Hückel reciprocal length parameter, which is calculated as 15 nm^{-1}. The Stern potentials between the sphere and the plate are then calculated based on the analysis of Behrens and Grier [15], where they regarded the charge of silica as localized entry on the surface and arising from a concentration of dissociated head groups. This basic Stern model illustrates that the counterions are separated from the surface by a thin Stern layer across which the electrostatic potential drops linearly from its surface value ψ_0 to a value defined as the diffuse layer potential ψ_d. This drop in the electrostatic potential is characterized by the capacity of the Stern layer, C. The diffuse layer Stern potential, for either 1 or 2, is written as a function of the charge density as follows [15]:

$$\psi_d(\sigma) = \frac{kT}{e}\ln\left(\frac{-\sigma}{e\Gamma+\sigma}\right) - (p\mathrm{H} - pK)\frac{kT}{e}\ln 10 - \frac{\sigma}{C} \quad (10)$$

The pH of the solution was measured as 6.5 by using a pH-meter (Corning Pinnacle Model 530). Using the surface charge density values of the tested particles given by the manufacturer (Molecular Probes, Inc.), the surface Stern potentials are calculated to be 44.4 mV for the glass substrate surface, 40.97 mV for $a=500$ nm, 24.89 mV for $a=250$ nm, 74.47 mV for $a=100$ nm, and 26.1 mV for $a=50$ nm.

However, there may be contributions to the total electrostatic potential other than the interactions based on equally spread charge on the sphere surface. One such may come from the trapped charges that are likely to form on the bottom of the insulating polystyrene sphere when it "jumps to contact" with the substrate [16]. When the sphere is in contact with the substrate, charge is free to flow in order to minimize the contact potential difference. In addition, the sphere deforms due to surface forces and touches the substrate over a finite area. The radius a_0 of this contact area can be estimated from the Johnson-Kendall-Roberts (JKR) theory [16] as $a_0 = 6\pi a^2 W/K$, where W is the work of adhesion given by $W = \gamma_1 + \gamma_2 - 2\sqrt{\gamma_1\gamma_2}$, and γ_1, γ_2 are the surface free energies of polystyrene and silica, respectively. The parameter $K\ [\equiv (4/3)(1-\nu_1^2/E_1 + 1-\nu_2^2/E_2)^{-1}]$ includes the elastic properties of the surface with ν_1, ν_2 being the Poisson ratios of polystyrene and glass substrates, respectively, and E_1 and E_2 being the Young's moduli for polystyrene and glass, respectively. The effective radius is now calculated to be $a_0 = 93$ nm for $a=500$ nm, 59 nm for $a=250$ nm, 37 nm for $a=100$ nm, and 20 nm for $a=50$ nm.

Since the electromotive force can be considered to be concentrated on the bottom area within the effective radius, calculations of the electrostatic potential incorporate the effective radius a_0 in Eq. (9) while retaining a in estimating the gravitational and van der Waals potentials. The total potential [Eq. (6)] for a particle located at h is given by

$$\phi(h) = \frac{4}{3}\pi a^3 g\Delta\rho h + \frac{A_{123}}{6kT}\left[\frac{1}{\delta} + \frac{1}{\delta+2} + \ln\left(\frac{\delta}{\delta+2}\right)\right] + 16\varepsilon a_0\left(\frac{kT}{e}\right)^2 \tanh\left(\frac{e\psi_1}{4kT}\right)\tanh\left(\frac{e\psi_2}{4kT}\right)e^{-\kappa h}. \quad (11)$$

Differentiating Eq. (11) with respect to h and then equating it to zero provides local minima corresponding to the equilib-

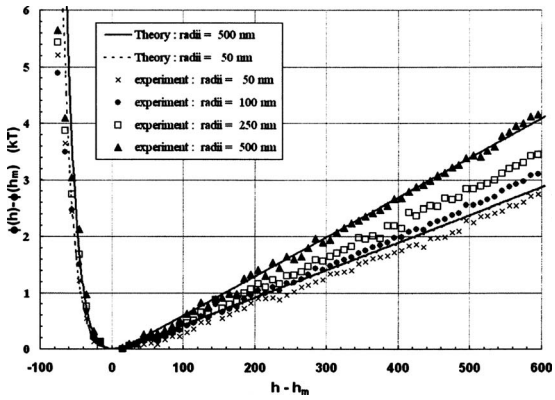

FIG. 3. Potential energy profiles for polystyrene spheres of various radius levitated above a cover glass. The curve fits have been constructed with $\Delta\rho=55$ kg/m^3, $A_{123}=-2.095k_BT$ nm^{-1}, $\kappa^{-1}=15$ nm, $a=50-500$ nm, $T=293$ K.

rium height (h_m), which is also called a separation distance. Experimentally measured particle-wall potentials have been determined from the correlation of the potential energy with the particle height location [2]. Figure 3 shows the potential energy profiles on a separation scale relative to the most probable height or the equilibrium height (h_m) used. Potential energy is reported on a scale relative to the minimum for each profile, $\phi_{\min}$, which inherently occurs at the most probable height as described by the Boltzmann equation. It is seen that there is an excellent agreement of the experimental data with Eq. (11).

Figure 4 shows the separation distances calculated using Eq. (11) and also shows the root mean square of the MSD predictions $\langle|z|\rangle$ ($\equiv\sqrt{2D_H\Delta t}$) represented by the extended bars centered at the corresponding equilibrium heights. Since the particles cannot penetrate the solid wall, the lower portions of the extended bars are shown by dashed lines, clearly manifesting that the near-wall Brownian motion should be further reduced beyond the simple hydrodynamic hindrance predictions, and the additional hindrance progressively increases with decreasing particle sizes. For the larger particles (250 and 500 nm radius), the "wall-interception hindrance"

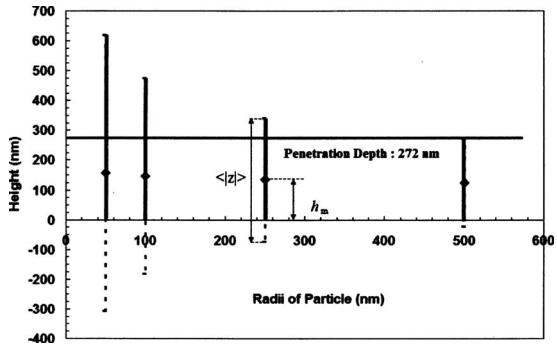

FIG. 4. Predictions of root mean square of MSDs, i.e., ($\langle|z|\rangle \equiv\sqrt{2D_H\Delta t}$), based on the near-wall hindrance by hydrodynamic slowdown [6,7], and estimated separation or equilibrium heights (h_m) for four differently sized nanoparticles.

is small and this is consistent with the findings of the noticeably small discrepancies between the measured and predicted MSD values as shown in Fig. 2.

In addition, the limited intensity of the evanescent wave field can result in a measurement system bias by underestimated measurements of MSD near the equilibrium heights. The horizontal dashed line in Fig. 4 shows the penetration depth (z_p) of the evanescent wave field at the fraction of e^{-1} of its intensity at the substrate surface. Because of the substantially reduced illumination intensity beyond the penetration depth, it is expected that the range of the Brownian displacements extending beyond z_p will not be effectively detected and the measurements can be systematically biased. The bias is expected to be great for smaller particles because of their larger Brownian displacements. Therefore, larger deviations of the data from theory should be partly attributed to the underestimated system bias. However, the solid-wall interaction associated with the equilibrium heights is believed to play a more decisive role for the discrepancies since it physically restricts the particle motion by the impermeable solid surface.

This work was supported by the U.S. Department of Energy, Office of Basic Energy Science, under Contract No. DE-FG02–05ER46182.

[1] A. Rohrbach, Biophys. J. **78**, 2641 (2000).
[2] D. C. Prieve, Adv. Colloid Interface Sci. **82**, 93 (1999).
[3] A. Banerjee and K. D. Kihm, J. Heat Transfer **126**, 505 (2004).
[4] S. Jin *et al.*, Exp. Fluids **37**, 825 (2004).
[5] K. D. Kihm *et al.*, Exp. Fluids **37**, 811 (2004).
[6] A. J. Goldman *et al.*, Chem. Eng. Sci. **22**, 637 (1967).
[7] H. Brenner, Chem. Eng. Sci. **16**, 242 (1967).
[8] M. Bevan and D. C. Preive, J. Chem. Phys. **113**, 1228 (2000).
[9] A. Einstein, Ann. Phys. **17**, 549 (1905).
[10] J. F. Brady and G. Bossis, Annu. Rev. Fluid Mech. **20**, 111 (1988).
[11] G. K. Batchelor, J. Fluid Mech. **52**, 245 (1972).
[12] H. H. Grünberg *et al.*, J. Chem. Phys. **114**, 10094 (2001).
[13] J. Israelachvili, *Intermolecular and Surface Forces* (Academic, London, 1992).
[14] S. L. Carnie *et al.*, Langmuir **10**, 2993 (1994).
[15] S. H. Behrens and D. G. Grier, J. Chem. Phys. **115**, 6716 (2001).
[16] B. Gady *et al.*, Phys. Rev. B **53**, 8065 (1996).